Proceedings of the Sixth International ASME Conference on Nanochannels, Microchannels and Minichannels
ICNMM2008
June 23-25, 2008, Darmstadt, Germany

ICNMM2008-62282

DSMC SOLUTION OF SUPERSONIC SCALE TO CHOKED SUBSONIC FLOW IN MICRO TO NANO CHANNELS

Ehsan Roohi
Email: roohi@ae.sharif.edu

Masoud Darbandi
Email: darbandi@sharif.edu

Vahid Mirjalili
Email: v.mirjalili@gmail.com

Department of Aerospace Engineering,
Sharif University of Technology,
P.O. Box 11365-8639, Tehran, Iran,

ABSTRACT

In this study, the supersonic and choked subsonic flows through micro/nano channels are investigated using direct simulation Monte Carlo (DSMC) method. The supersonic case is simulated at different Knudsen numbers covering slip to transition flow regimes, while the effects of inlet Mach and back pressure are studied in details. The inlet/outlet pressure boundary conditions are suitably implemented benefiting from the basics of characteristics theory. A behavior similar to the one predicted by the Fanno theory is observed here; i.e., the supersonic flow velocity decelerates up to a choking condition where any further increase in Knudsen number is impossible unless strong normal/oblique shocks appear at the inlet and the inlet conditions change to the subsonic ones. However, a subsonic flow appears near the outlet section if one imposes a back pressure lower than the ordinary exit pressure at the outlet. Our investigation showed that applying the back pressure boundary condition right at the real channel exit would overwhelm the solution. A more realistic behavior can be achieved by inserting suitable buffer zone beyond the real channel exit, where the back pressure is applied there. This strategy results in capturing a more realistic physics of flow at the channel outlet and enforces choking condition at the outlet.

1. INTRODUCTION

Micro and nano channel applications are widely observed in Micro Electro Mechanical Systems (MEMS), hence, the flow analysis in MEMS is becoming increasingly important. In order to enhance the design and performance of such systems, a deeper understanding of flow and heat transfer is normally required in them. Previous investigations [1-2] have proven that the flow behavior in MEMS is different from that in macro systems. The mini, micro and nano channels in MEMS may work in a variety of flow regime conditions such as the continuum, slip, and transition ones, see Fig. 1. As is indicated in this figure, the main characteristic to determine gas rarefaction has been the Knudsen number; which is defined as the ratio of the mean free path of the fluid to the characteristic dimension of the channel ($Kn=\lambda/H$). For the flows with small Knudsen numbers, i.e., $Kn<0.01$, a continuum assumption is justifiable. In such flows, the analysis can be fulfilled via solving either the Euler equations for inviscid flows or the Navier-Stokes equations for viscous flows. For flows with Knudsen numbers between 0.01 and 0.1, the non-equilibrium effects dominate in the flow near the wall surfaces, which can properly be described by applying new boundary conditions such as the velocity slip and temperature jump conditions to solve the Navier-Stokes equations. For flow with a Knudsen number greater than 0.1, high order kinetic effects become important and the linear stress-strain relationships in the Navier-Stokes equations become invalid.

If the Knudsen number is further increased, the flow characteristics become significantly different from the equilibrium ones. Hence, the computational models have to be established based on the kinetic principles such as those in the Boltzmann equation. As is known, the Navier-Stokes equations can be derived from the Boltzmann equation under the assumption that small departure of the distribution function from equilibrium is permitted. Therefore, they become unsuitable for studying rarefied flows, where the distribution function is considerably non-equilibrium in nature. The exact solution of the Boltzmann equation exists only for a limited number of free-molecular flows and simple geometries. Thus, the non-equilibrium gas flow problems occurring in complex

geometries should be solved only via the numerical solutions of the Boltzmann equation. The complexity in Boltzmann equation (due to its multi dimensionality in time, three space coordinates and three velocity components) suggests the use of direct simulation Monte Carlo (DSMC) techniques to obtain numerical solution for this equation. As is known, the DSMC is one of the most successful particle simulation methods, which has been widely used in analyzing the rarefied gas flows [3].

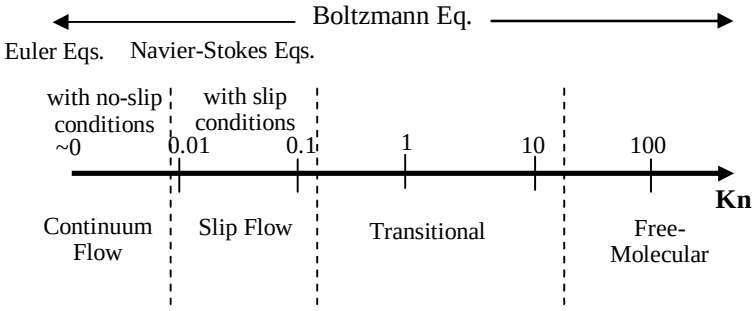

Figure 1. The flow treatment at different Knudsen numbers.

Different applications of DSMC have been reported to simulate supersonic microflows [4-8]. Oh et al. [4] coupled DSMC with monotonic Lagrangian grid (MLG) to study the flow behavior in micro channels. The MLG is a general data structure in which the nodes represent the particles. They specified the back pressure at the outlet boundary benefiting from a virtual region outside the computational domain. They simulated the flow at three Knudsens of 0.07, 0.14, and 0.19. Their results showed that the downstream development of flow variables would qualitatively follow the basics of Fanno theory. They found that the velocity slip and temperature jump would increase at the channel entrance as Kn was increased. Contrary to the wall temperature jump, the velocity slip did not change in the downstream. Liou and Fang [5] also studied the heat transfer characteristics of supersonic flows in microchannels using DSMC. They applied the variable hard sphere (VHS) model [3] to simulate the molecular collision. The results showed that the magnitude of the temperature jump and the heat transfer to the isothermal wall would increase as Kn was increased. They also showed that the enhanced wall heat transfer would be mainly caused by the increase rate of molecules impacting the wall.

Le and Hassan [6] and Le et al. [7] studied the flow behavior and heat transfer characteristics in high speed gas flows through two-dimensional microchannels via applying zero and non-zero back pressures. It was observed that the subsonic flow would appear near the outlet region if the applied back pressure was lower than the ordinary exit pressure in a full supersonic situation. Additionally, the flow temperature and wall heat transfer increased rapidly at the channel outlet. Titove and Levin [8] used a collision limiter method called equilibrium direct simulation Monte Carlo (eDSMC) to simulate high pressure flows in nozzle and embedded-channels. Providing sufficient number of collisions, the eDSMC method captured appropriately the simple inviscid compressible flow field behavior. However, the comparison of eDSMC results with those of an exact DSMC flow field showed that the approximation of equilibrium would be inadequate for the viscous boundary layer part in the nozzle. They concluded that eDSMC would be an alternative to solve the Euler equations and potentially an alternative to the NS equations for high pressure flows with small viscous regions.

In this study, standard DSMC approach is used to simulate supersonic micro/nano channel flows applying zero and non-zero back pressure conditions. The objective of this work is to study more details of flow in micro and nano scale channels and to investigate the back pressure effects on this behavior. We also discuss the correct position where the back pressure should be applied. Finally, we describe the subsonic choked flow in pressure driven micro-nano channels and discuss the ways that the correct physics of flow can be simulated numerically. Contrary to the past references [4-8], which do not describe the importance of the buffer zone in details, this paper studies the effects of back pressure, the correct position of back pressure implementation, and the importance of the buffer zone in details.

2. GOVERNING EQUATIONS

2.1 Velocity distribution function and the Boltzmann equation

To formulate the molecular motions in a flow, Maxwell suggested a velocity distribution function $f(c)$ to describe the probability of a molecule to have a certain velocity at a certain location and a specific time. Due to molecular chaos in a dilute gas, it is possible to use a velocity distribution function for a single molecule. Other macroscopic quantities can be calculated using this velocity distribution function. The Boltzmann equation, which describes the time evolution of the velocity distribution function of molecules, is given by

$$\frac{\partial}{\partial t}(nf) + c\frac{\partial}{\partial r}(nf) + F\frac{\partial}{\partial c}(nf) = \int_{-\infty}^{\infty}\int_{0}^{4p} n^2(f^* f_1^* - ff_1)c_r s \, d\Omega dc_1 \quad (1)$$

where n is number density, t is time, r is space vector, c is velocity space vector, F is external force per unit mass, c_r is the relative velocity between a molecule of velocity class c and one with velocity class c_1 , $\sigma \, d\Omega$ is differential cross-section for the collision of a molecule of class c with another one having class c_1 such that their post-collision velocities are c^* and c_1^*, respectively, and functions f, f_1, f^* and f_1^* are the corresponding velocity distribution functions for the molecule and its collision partner before and after the collisions. Equation (1) is a seven-dimensional integro-differential equation. The first term describes the change rate of the number of molecules. The second and third terms describe the changes of the number of molecules due to molecular movement and due to an external force field. The term on the right-hand-side is called the collision integral term, which causes major difficulty to solve this equation. This term describes the change of molecular velocities after molecular collisions.

2.2 The DSMC approach

The direct simulation Monte Carlo (DSMC) method [3] is a numerical tool to solve the Boltzmann equation based on direct statistical simulation of the molecular processes described by kinetic theory. This method is considered as a particle method to simulate the particles behavior. Each particle represents a large bulk of real gas molecules. The primary

principle of the DSMC method is to decouple the motion and collision during a time step Δt into two sequential stages of free-molecular movement and then collision. Implementation of the DSMC method requires breaking down the computational domain into a number of grid cells. The size of each cell should be small enough to result in small changes in thermodynamic properties across each cell. The cells are divided into sub-cells in each direction. Sub-cells are then utilized to facilitate the selection of collision pairs. The time step is selected as $\Delta t = \min(t_{col}; t_{res})$, where t_{col} is the mean collision time and t_{res} is the mean residence time. In another words, the molecules in each cell do not cross more than one cell during one time step. After fulfilling all molecular movements, the collisions between molecules are simulated in each cell independently. In the current study, the VHS collision model is used and the choice of collision pair is done based on the no time counter (NTC) method. NTC scheme makes the computational time proportional to the number of the simulated particles [3].

The following procedure is used to solve a stationary problem with DSMC. In the entire computational domain, an arbitrary initial state of gas is specified and the desired boundary conditions are imposed at time zero. After achieving steady flow condition, sampling of molecular properties within each cell is fulfilled during sufficient time period to avoid statistical scattering. All thermodynamic parameters such as temperature, density, and pressure are then determined from this time-averaged data.

2.3 Inlet and outlet boundary conditions

2.3.1 Supersonic Flow

The one-dimensional wave theory indicates that there are three incoming characteristic waves, which propagate the information into the channel at the inlet. In a supersonic flow the inlet Mach number, temperature and density are specified at the inlet. All outlet variables are extrapolated during numerical procedure. On the other hand, in numerical simulation of flow with a specified pressure (P_e) at the channel outlet, special boundary condition treatment is required with one incoming characteristic wave at the outlet. In the DSMC method, all three flow parameters, i.e., density, temperature and velocity must be specified for incoming molecules at the inlet/outlet boundaries. Therefore, the temperature and velocity must be approximated using the information from the interior domain. In this regard, we can utilize the 1-D characteristic theory [5, 9]. For a backward-running wave, we consider $du/a = -d\rho/\rho$, where r is mass density and $a^2 = (dP/d\rho)$ is the speed of sound. Applying the definition of the speed of sound in a differential form to a boundary cell, it yields

$$(r_e)_j = r_j + \frac{P_e - P_j}{a_j^2} \tag{2}$$

The subscripts e_j represent the quantities at the cell j adjacent to the outlet boundary. The temperature at the outlet can be found from the ideal gas law, as it follows

$$(T_e)_j = P_e / ((r_e)_j R) \tag{3}$$

The velocity is also computed from the characteristic wave equation, i.e.,

$$(u_e)_j = u_j + \frac{P_j - P_e}{r_j a_j} \tag{4}$$

Equations (3)-(4) determine the temperature and velocity at the outlet using the pressure value. They are called Whitfield's characteristic formulation [10].

2.3.2 Subsonic Flow

For a subsonic pressure driven flow, the inlet velocity is also unknown and must be extrapolated from the interior magnitudes. Following Wang and Li [11], the inlet velocity is calculated from

$$(u_{in})_j = u_j + \frac{P_{in} - P_j}{r_j a_j} \tag{5}$$

and the density is calculated from the equation of state, i.e.,

$$(r_{in})_j = \frac{P_{in}}{RT_{in}} \tag{6}$$

2.4 Wall & Symmetry boundary conditions

The channel walls are treated as diffuse reflectors using the full thermal accommodation coefficient with a unit magnitude for a. The velocity of reflected molecules is randomly attributed according to one half-range Maxwellian distribution, which is determined by the wall temperature as it follows

$$\begin{aligned} u &= \sqrt{-\log(RF(0))}V_{mpf} \sin(2p \cdot RF(0)) \\ v &= \pm\sqrt{-\log(RF(0))}V_{mpf} \\ w &= \sqrt{-\log(RF(0))}V_{mpf} \cos(2p \cdot RF(0)) \end{aligned} \tag{7}$$

where $V_{mpf} = \sqrt{2RT}$ is the most probable speed of the molecules at the wall temperature and $RF(0)$ is a uniformly distributed random fraction between 0 and 1. The positive and negative symbols correspond to the lower and upper walls, respectively, k is the Boltzmann constant, and m is the molecular mass.

Reflection from symmetry boundary is considered specular, i.e., the normal velocity component is being reversed while the tangential component remains unchanged.

2.5 Initial Conditions & Convergence

At time zero, 7–16 molecules are set in each cell. Each of them has a thermal velocity and a randomly defined location. The number of simulated particles should be large enough to prevent any apparent fluctuation, however not too large to exceed the limiting computational capabilities.

For pressure driven subsonic flows, an initial velocity field (U_{initial}) is required to start the calculations. We choose U_{initial}=100 m/s. Similar to the conclusions presented in Ref. [5], we also observed that the choice of initial inlet velocity has no impact on the final solution, nevertheless, the correct inlet velocity, corresponding to the specified pressure ratio, would be found as the solution converges.

Time step for computation is calculated such that the CFL number ($CFL = \frac{V_{mpf}\Delta t}{\Delta x_{cell}}$) remains less than 0.1. The value of mass flow rate from inlet and outlet are monitored until there is no difference between the inlet and outlet mass flow rates. The computation is continued long after this situation to suppress inherent statistical fluctuations in DSMC.

3. RESULTS AND DISCUSSION

We study different cases in order to elaborate flow behavior in our chosen micro-nano channels. They are summarized in Table 1. In all of our studies, we consider nitrogen as the working fluid. In order to apply the boundary conditions precisely, it is suggested that two buffer regions be added at the inlet and outlet of the channel [12]. In the current study, we use the buffer region either at the inlet or outlet and then compare the results with the other simulations, where there are no buffer zones. In order to investigate the effect of downstream boundary condition comparatively, some of the studied cases are similar to simulations performed in Refs. [6-7]. The channel geometry is schematically shown in Fig. 2. One half of the geometry is simulated due to the symmetry.

Table 1. The chosen test cases and their details

Case	1	2	3	4	5	6	7	8 (a)-(b)	9
H (μm)	10.0	8.35	0.7	0.6	1.2				1.35
AR (L/H)	5								6.66
Kn_{in}	0.062		0.43		0.062				0.074
M_{in}	4.15							3.39	Not fixed
Buffer	I.	O.	Not used						O.
Grid	120×60		100×60						120×60
P_b (Pa)	V.	0.0			V.	0.5 M	0.7 M	V	0.5 M	6.73 k
PR	Not fixed								15
T_{in},T_w	300, 323								

I.: Inlet,
O.: Outlet,
V.: Vacuum,
PR: Pressure ratio

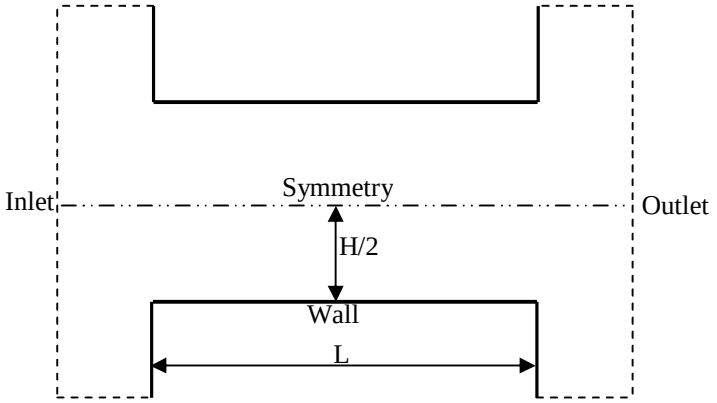

Figure 2. The geometry of channel imposed by inlet/outlet buffer zones

The computational domain consists of two rectangles; the main channel and the buffer region, which were discritized with 100×40 and 20×60 structured cells, respectively. The chosen number of cells was finalized after a careful grid refinement study. Each cell is subsequently divided into 2 sub-cells in each direction. The size of each cell is lower than the mean free path (l) in both x and y directions. For example, the cell sizes in case 1, where $l = 62\times10^{-8}$, are $\Delta x_{cell} = 50.22\times10^{-8} = 0.81l$, $\Delta y_{cell} = 16.74\times10^{-8} = 0.27l$.

The Knudsen number can be related to the Reynolds and Mach numbers via

$$Kn = \sqrt{\frac{gp}{2}}\frac{M}{\mathrm{Re}} \qquad (8)$$

For all the simulated cases in this study, Reynolds number is less than 10, hence, the flow is highly dominated by viscous forces. Consequently, increasing the value of Kn leads to viscous force increase. In order to simulate the free stream condition correctly in the current work, 10% of the wall length at the entrance region of the channel is considered as a specular reflector.

3.1 Supersonic flow

3.1.1 Global characteristics

A. cases 1 and 2

Mach contours for case 1 are shown in Fig. 3. In this case, the supersonic flow faces two bow shock waves in front of the walls before entering the channel. These shocks cross each other in the channel somewhere at x=22 microns. This results in diffusive waves, which gradually disappear in the downstream due to high viscous forces. The viscous force is strong enough to prevent the reflection of incident oblique shocks to reach the channel walls. It should be noted that there are convective force, shear stress and wall heat transfer in channels with isothermal wall conditions which form the physics of flow. After the appearance of the shocks, the main flow gets hotter than the walls; therefore, there is heat transfer from the flow to the wall. From basic Rayleigh theory, this heat transfer may increase the Mach. Meanwhile, the shear stress is much stronger in this scale and therefore can retard the flow. As the flow moves downstream, the rate of heat transfer decreases and shear forces reduce the Mach more effectively, see Fig. 7. As the flow approaches the outlet, there is an expansion in that the flow approaches the ambient with much lower pressure. This expansion is followed by an increase in Mach and cooling of the flow.

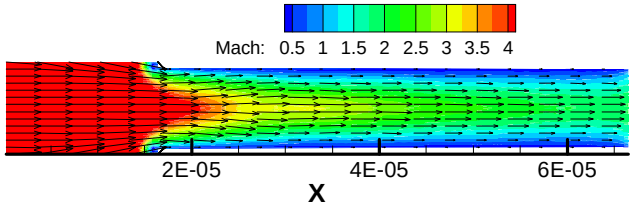

Figure 3. Case 1, Mach contours, Kn_{in}=0.062, M_{in}=4.15, and applying vacuum boundary condition.

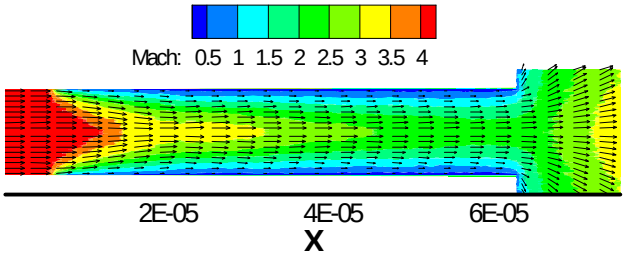

Figure 4. Case 2, Mach contours, considering Kn_{in}=0.062, M_{in}=4.15, and P_b=0

In the next step, we consider the effect of outlet buffer zone in our solution. For the studied cases 1 and 2, the viscous effects are not strong enough to retard the supersonic flow to choking condition or change the upstream condition to subsonic condition. Therefore, any type of pressure setting at the downstream end of buffer zone does not influence the flow in upstream channel. The occurrence of expansion at the outlet of the channel is clearly visible in Fig. 4.

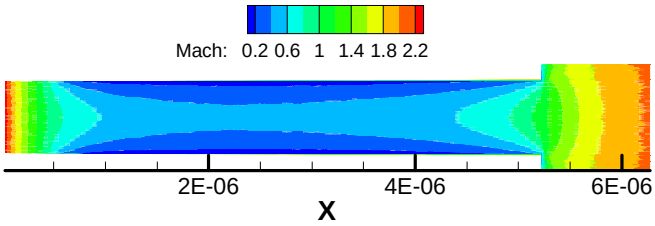

Figure 5. Case 3, Mach contours, Kn_{in}=0.43, M_{in}=4.15, and P_b=0

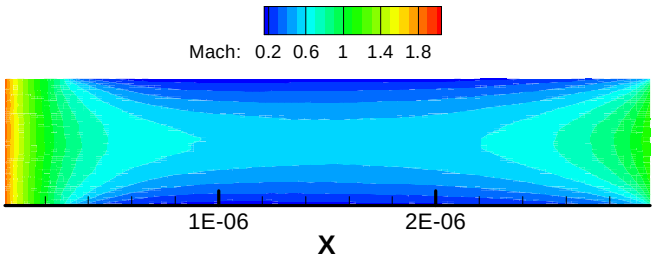

Figure 6. Case 4, Mach contours, Kn_{in}=0.43, M_{in}=4.15, and applying vacuum boundary condition.

B. Cases 3 and 4

In this step, we consider the flow in transition regime, where Kn_{in}=0.43. Comparing to the pervious test cases, Reynolds number decreases and the viscous forces become more dominant. Simulations are performed for the channel geometry with and without the buffer zone at the outlet and the results are shown in Figs. 5-6. It is observed that the resulting friction force is strong enough to change the upstream condition via normal/oblique shock waves at the specular reflector portion at the channel inlet. From Fanno theory, which corresponds to friction dominated flow in constant area ducts, it is known that if the channel becomes longer than a specific length, which corresponds to the choking condition, the flow changes the upstream condition. It changes the flow regime from a supersonic condition to subsonic one to meet the correct mass flow rate into the domain. Therefore, for the current inlet setting (Mach, Knudsen), it is impossible to have supersonic flow with an inlet setting of M_{in}=4.15. The velocity of subsonic flow decreases and minimum Mach occurs at *X/L*=0.4 for both cases 3 and 4. The low variation of flow velocity at the core region of the channel, *X/L*=0.3-0.65 may be attributed to the reverse effects of heat removal from the subsonic flow, which decelerates the flow, and the viscous force, which accelerates it. The balance of these two forces makes the velocity variation small until *X/L*=0.65, where the flow starts expanding there. This is due to the reduction of heat removal from the mean flow; therefore, the flow starts accelerating by viscous forces. Mach increases up to 1.10 at the exit for the channel with buffer zone and to 1.21 for the channel without buffer. The basic aspects of rarefied gas flow are clearly observed in this highly non-continuum flow. First, the change from supersonic to subsonic flow is attributed to the oblique shocks, which emanate from the boundary layer after the normal shocks, which have already reduced the Mach from one supersonic condition to another one. Second, the subsonic flow expands to weak supersonic flow at the outlet. These features can be attributed to the strong effects of viscosity in micro-nano scales and have been confirmed by other researchers as well [13]. We have to emphasize on the importance of the buffer zone to fix the back pressure for the situation where the flow remains subsonic. It should be noted that a fixed back pressure does not influence the main channel flow when the flow becomes supersonic at the outlet.

Figure 7 shows the Mach distribution at the channel centerline for three different inlet settings of Kn=0.062, 0.35, and 0.43 and M_{in}=4.15. Similar to case 3, the flow with Kn=0.35 decelerates to subsonic condition and remains subsonic until the flow reaches near the channel exit, where it turns to slight supersonic condition. The viscosity effects are more pronounced for Kn=0.43 case, where the inlet Mach decreases from 4.15 to 2.35.

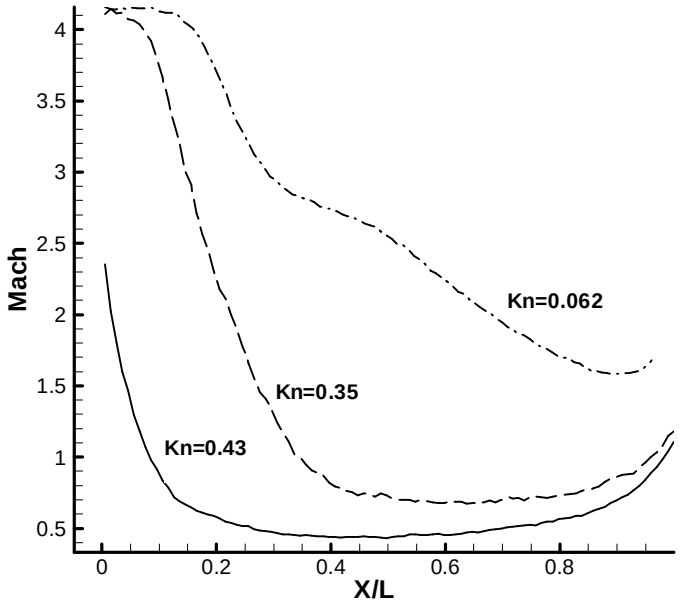

Figure 7. Comparison of Mach distribution for three different inlet Knudsen numbers; M_{in}=4.15 and P_b=0

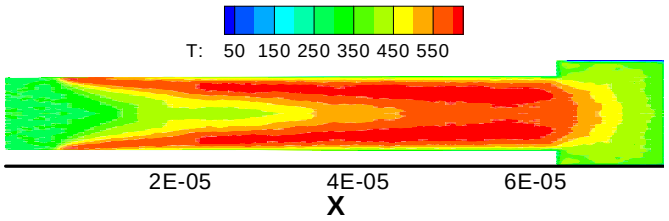

Figure 8. Case 2, temperature contours; Kn_{in}=0.062, M_{in}=4.15, and P_b=0

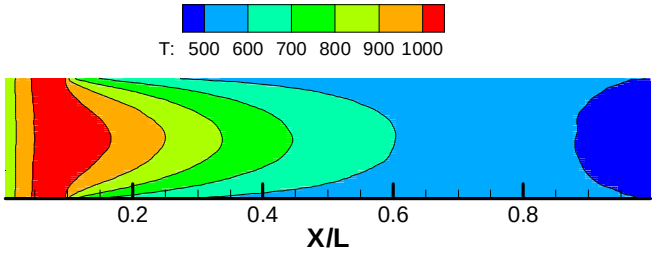

Figure 9. Case 4, temperature contours; Kn_{in}=0.43, M_{in}=4.15 and applying vacuum boundary condition

The temperature contours for cases 2 and 4 are shown in Figures 8 and 9, respectively. As is observed, there are different behaviors for the supersonic-subsonic flow cases. For case 2, there is a gradual increase in temperature just after the oblique shocks. Consistent with Fanno theory, the temperature increases along the channel. This can be attributed to the conversion of kinetic energy to internal energy. On the other hand, the strong shocks at the entrance of the channel highly increase the flow temperature when Kn=0.43. As the subsonic flow accelerates in the channel, the temperature decreases and the flow cools down due to heat transfer to the channel wall, which has a lower temperature than that of the mean flow. There is again a slight decrease of temperature (from 301 to 296 Kelvin) just at the channel exit as soon as the flow turns to supersonic flow condition.

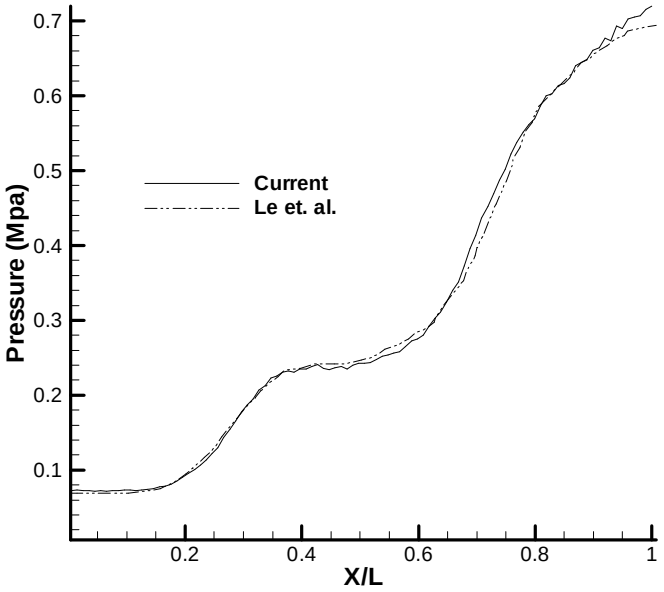

Figure 10. Case 7, centerline pressure distribution along the channel, Kn_{in}=0.062, M_{in}=4.15, and P_b=0.7 MPa, and comparison with Le et al. [7]

3.1.2 Effect of back pressure

C. Cases 5-8

In this section, we study the effects of imposing a back pressure other than the vacuum or P_{out}=0 at the channel outlet. Figure 10 shows the pressure distribution along the channel centerline for the case with Kn=0.062, M_{in}=4.15, and P_{out}=0.7 MPa and compares it with the result of Le et al. [7]. There is good agreement between them. The first peak in pressure distribution is due to the appearance of an oblique shock at the channel entrance. There is a region of constant pressure in the channel (X/L=0.30-0.57) followed by a gradual increase of pressure up to points very close to the exit region. This pressure increase cannot be attributed to another shock, but to the reflection of waves from the corresponding boundary layer.

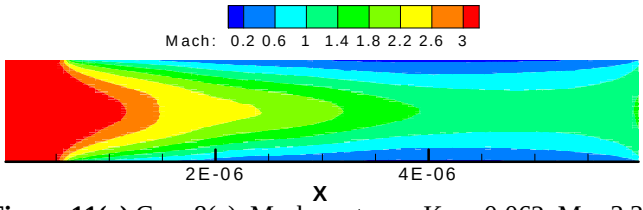

Figure 11(a) Case 8(a), Mach contours; Kn_{in}=0.062, M_{in}=3.39, and applying vacuum boundary condition

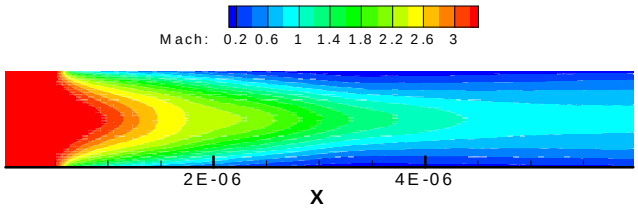

Figure 11(b) Case 8(b), Mach contours; Kn_{in}=0.062, M_{in}=3.39, and P_b=0.5 MPa

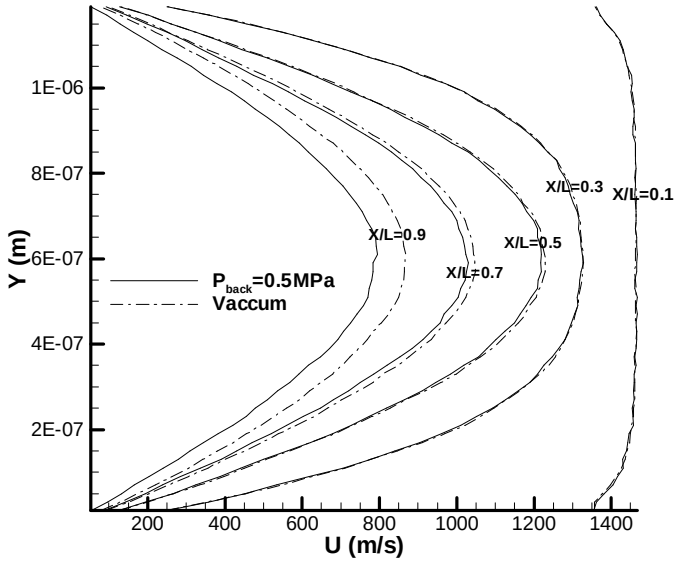

Figure 12. Cases 5 & 6, velocity profiles at different positions along the channel with Kn_{in}=0.062, M_{in}=4.15, and imposing vacuum and non-vacuum boundary condition, P_b=0.5 MPa

Mach contours for cases 8(a) and 8(b), which have a lower inlet Mach (M_{in}=3.39) comparing with the preceding cases, are shown in Figs. 11 (a)-(b). Near the inlet of the channel, both cases show similar behavior, however, the flow characteristics become different in the rest of domain. The imposed back pressure highly decreases the Mach number inside the channel, as is observed in Fig. 11(b). One characteristic of the rarefied flow can be observed in case 8(b) as the exit Mach drops below 1, i.e., M_{exit}=0.86. Meanwhile, it is higher than 1 in case 8(a), i.e., M_{exit}=1.41. The imposed back pressure does not permit the expansion waves to occur at the outlet; consequently, the patterns of Mach contours are different from case 8-(a).

Therefore, we conclude that the imposed back pressure in addition to high viscous forces could slow down the supersonic condition to subsonic one in micro-nano scales.

To study the effects of back pressure on the velocity distribution, the velocity distributions for two cases 5 and 6 with vacuum and 0.5 MPa imposed back pressure are shown in Figure 12. There is no influence of the imposed pressure in the regions before (*X/L*=0.6), hence, the velocity profiles are identical. However, the back pressure starts affecting the main flow after this region and therefore, the velocity slows down more as it approaches the channel exit in case of P_b=0.5 MPa.

3.2 Choked Subsonic flow

Several studies on subsonic flow treatment using the DSMC technique have been reported in past [12, 14-15]. However, there are few investigations to study the choked flow. In this section, we study choked subsonic flow and carefully evaluate the effect of specifying the back pressure at different positions. Figure 13 (a)-(e) shows the results for case 9, which corresponds to subsonic flow with Kn_{in}=0.146 and PR=15. Figure 13(a) shows the Mach contours for a pressure driven channel, where the back pressure is applied just at the outlet. However, Figure 13(b) presents the results when the back pressure is applied at the end of the inserted buffer zone. The longitudinal and transversal sizes of buffer zone are 20% of the channel length and 133% of the channel height, respectively. Since the applied pressure ratio is much higher than that of the choking condition, i.e., 5.26, enforcing an overwhelmed back pressure just at the outlet of the channel leads to incorrect velocity (Mach) at the outlet. It means that it leads to a supersonic Mach (M=1.15) at the outlet. It can be concluded from Eqs. (2-4) that the velocity of molecules adjacent to the outlet boundary and the thermodynamic properties of the cells located near the outlet are directly influenced by the exit pressure. Once the choking occurs, the exit pressure does not drop any further. Therefore, applying the back pressure (which is much lower than the exit pressure) just at the channel outlet results in a physically incorrect solution. Additionally, the number density of entering molecules depends on the velocity magnitude and is computed from

$$n = \frac{n}{2\sqrt{pb}}[\exp(-s^2\cos^2 q) - \sqrt{p}\, s\cos q\{1 - erf(s\cos q)\}]$$
$$s = \frac{u}{V_{mpf}}, q = 180 \qquad (9)$$

Therefore, enforcing a too low back pressure, i.e., less than the limiting value for choking condition, would falsely reduce the number of molecules entering into the domain from the outlet section because of incorrect velocity. To implement the physics of flow properly, we apply the back pressure at the end of buffer region and the real solution is permitted to be self adjusted at the outlet, see Fig. 13(b). This results in capturing a sound physical Mach number (M=1) at the outlet section. Due to the strong wall's friction, the sonic condition appears right at the centerline [12]. Figure 13(c) shows the pressure distribution along the channel. The pressure varies only in the streamwise direction and there are little changes in the transversal direction. The isotherms and the centerline Mach, temperature and pressure distributions are shown in Figs. 13 (d)-(e). The temperature field can be divided into three regions. At the inlet, there is a heating from the wall to the mean flow due to higher temperature of the wall. In this region, this heat transfer to the subsonic flow increases the effects of viscous force which acts as a driving force for subsonic flow. Once the temperature of the flow approaches to that of the wall, at $X/L \approx 0.35$, the heat transfer decreases and the flow speeds up by shear stress. This process is followed by decrease in temperature until the end of the channel, see Fig. 13-e. Due to the strong rarefaction effects, the pressure distribution (non-dimentionalized with its corresponding inlet value) is slightly non-linear [16]. Most of the changes in Mach (or velocity) occur at the last 20% region of the channel in which Mach increases from 0.45 to 1. It should be noted that the outlet Kn reaches to a value about 0.388, which indicates that the flow is completely in transition regime.

Graur et al. [17] derived an analytical expression for mass flow rate in long microchannel under isothermal condition. It is given by

$$Q = \frac{H^3 p_0^2}{24 m RTL} F(\Pr, k_l, kn_o),$$
$$F(\Pr, k_l, kn_o) = \Pr^2 - 1 + 12 kn_o(\Pr - 1) + \frac{24}{k_l^2} kn_o^2 Ln(\Pr) \qquad (10)$$

, where R is the universal gas constant, L is the channel length, H is the channel height, P_o is the outlet pressure and m is the viscosity coefficient. The value of k_λ is 1.03 for nitrogen under the VHS model assumption [3]. If we use the choking pressure ratio, i.e., *PR*=5.26 in Eq. (9), it gives a value of 0.69×10^{-5} *kg/(ms)* for mass flow rate. Karniadakis et al. [16] suggested another expression to predict the mass flow rate in micro-channels as it follows

$$Q = \frac{H^3 p_0 (p_i - p_0)}{24 m RTL}[(\Pr+1) + 2kn_o(6 + \bar{a}) +$$
$$12\frac{b + \bar{a}}{\Pr - 1} kn_o^2 Ln(\frac{\Pr - bkn_o}{1 - bkn_o})], \quad b = -1, \quad \bar{a} = 2.2 \qquad (11)$$

For the setting in case 9, this equation predicts a value of 0.74×10^{-5} *kg/(ms)* for mass flow rate. Both of Eqs. (10)-(11) do not show any asymptotic behavior with pressure ratio. Hence, using the applied pressure ratio, *PR*=15, which is much higher than the choking pressure ratio, is inappropriate. Meanwhile, the current DSMC simulation predicts a value of 4.6×10^{-5} *kg/(ms)* for the mass flow rate, much higher than prediction given by analytical relations.

Under the assumption of isothermal flow in microchannels, a unified velocity model was suggested by Karniadakis et al. [16] to calculate the velocity profile in microchannels at all *Kn* regimes. It is given by

$$U^*(y, Kn) = U(x,y)/\bar{U}(x) = [\frac{\frac{y}{h} - (\frac{y}{h})^2 + \frac{Kn(x,y)}{1 - bKn(x,y)}}{\frac{1}{6} + \frac{Kn(x,y)}{1 - bKn(x,y)}}], b = -1 \qquad (12)$$

, where $\bar{U}$ is the mean velocity in the channel. Assuming negligible convective forces in long micro channels, Darbandi and Vakilipour [18] derived an expression for non-dimensional velocity profile based on the first-order wall slip boundary condition

$$U^*(y, Kn) = 6[\frac{\frac{y}{h} - (\frac{y}{h})^2 + Kn(x,y)}{1 + 6Kn(x,y)}] \qquad (13)$$

Equations (12)-(13) present analytical relations for velocity in rectangular channels as in isothermal flow condition.

Therefore, they are only applicable to low speed subsonic flows and are not valid for high speed supersonic flow calculations.

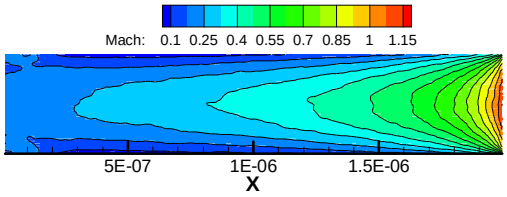

a) Contours of Mach (without buffer zone)

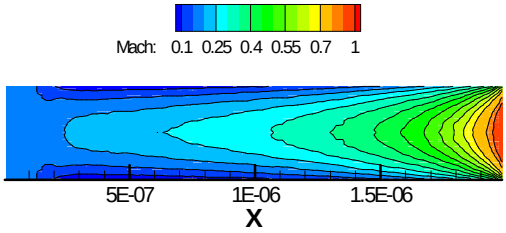

b) Contours of Mach (with buffer zone)

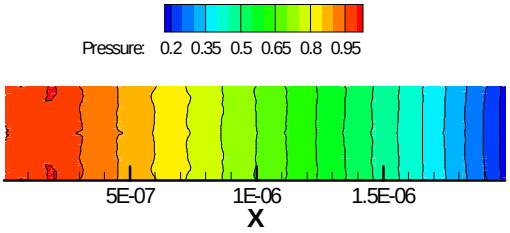

c) Contours of pressure

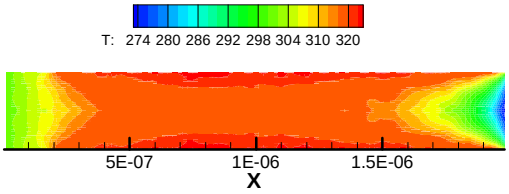

d) Contours of temperature

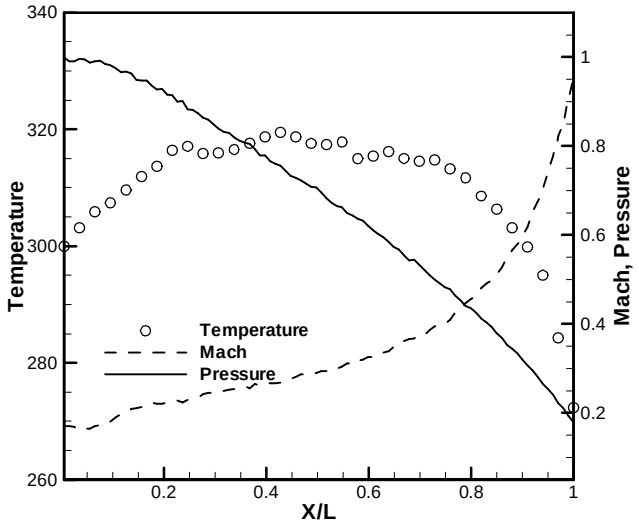

e) Distribution of temperature, Mach and pressure at a Pressure Ratio=15, Kn_{in}=0.146,

Figure 13. (a-e) Contours and distribution of parameters related to case 9

Figure 14 shows the velocity distributions obtained from DSMC for case 9 and the analytical expressions presented in Eqs. (12)-(13) at two cross sections of *X/L*=0.3 and 1. There is a general agreement between DSMC and both expressions at *X/L*=0.3, but there are some discrepancies among them at *X/L*=1. Consistent with the results reported in Ref. [16], it is observed that the unified model, Eq. (12), slightly overestimates the velocity slip at the walls. This overestimation is more pronounced if we compare the DSMC data with Eq. (13) at *X/L*=0.3. At the exit of the channel, both models anticipate poor estimation of velocity because the underlying assumptions on which they are derived are fully invalid, i.e., the flow is not isothermal at the exit at all, see Fig. 13-(e), and the convection force is not negligible, i.e. choking occurs.

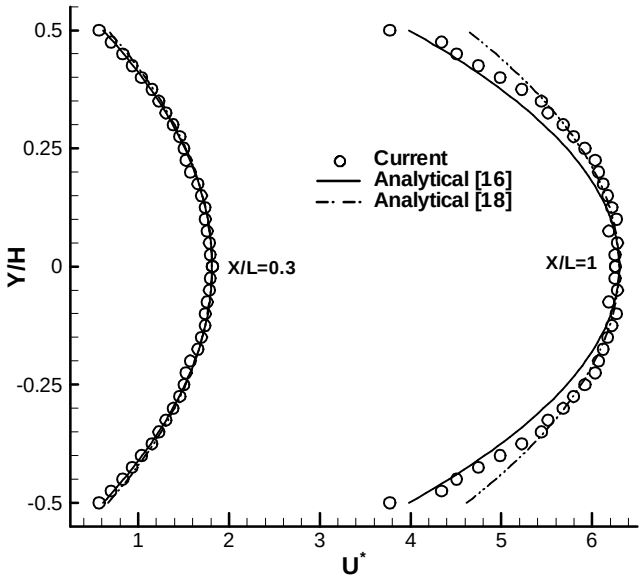

Figure 14. Comparison of DSMC velocity profiles for case 9 at *X/L*=0.3 and *X/L*=1 with analytical models of Karniadakis et al. [16] and Darbandi and Vakilipour [18]

4. Conclusion

Supersonic and subsonic choked flow in micro/nano channels were simulated using DSMC. The rarefaction effects were clearly observed in the mixed supersonic-subsonic flow regimes in the channel. The complex behavior of the rarefaction was due to strong viscous forces, which were dominant in the channel. To derive physical solutions, it was suggested to implement the back pressure at a buffer zone far from the channel exit even for full supersonic flow because it is possible that the viscous force changes the upstream condition via strong normal/oblique shock waves at the inlet. The role of buffer zone is more pronounced in the simulation of the subsonic flow with friction choking. It is because applying a non-physical pressure just at the channel exit results in incorrect velocity for the molecules entering to the domain and therefore wrong solutions are obtained.

ACKNOLEGMENT

The authors would like to express their gratitude to X. Chong from Institute of Mechanics of the Chinese Academy for helpful comments.

REFERENCES

[1] Arkilic, E., Schmidt, M. A., Breuer, K., 1997, Gaseous slip flow in long microchannels, Journal of Microelectromechanical systems, Vol. **6** (2), pp. 167-178.

[2] Ho, C., Tai, Y., 1998, Micro-electro-mechanical systems (MEMS) and fluid flows, Annual Review Fluid Mechanics, Vol. **30**, 579–612

[3] Bird, G. A., 1994, Molecular Gas Dynamics and the Direct Simulation of Gas Flows, Clarendon, Oxford.

[4] Oh, C.K., Oran, E.S., and Cybyk, B.Z., 1995, Microchannel flow computed with DSMC-MLG, AIAA paper 95-2090.

[5] Liou, W. W., and Fang, Y. C., 2000, Implicit Boundary Conditions for Direct Simulation Monte Carlo Method in MEMS Flow Predictions, Computer Modeling in Engineering & Science, Vol. **1**, pp. 119–128.

[6] Le, M., Hassan I., 2006, Simulation of heat transfer in high speed microflows, Applied Thermal Engineering, Vol. **26**, pp. 2035–2044.

[7] Le, M., Hassan I., Esmail N., 2007, The effects of outlet boundary conditions on simulating supersonic microchannel flows using DSMC, Applied Thermal Engineering, Vol. **27**, pp. 21–30.

[8] Titove, E. V., Levin, D. A., 2007, Extension of DSMC method to high pressure flows, International Journal of Computational Fluid Dynamics, Vol. **21** (9-10), pp. 351-368.

[9] Alexeenko A., Gimelshein S. F., Levin D. A., 2005, Reconsideration of Low Reynolds Number Flow-Through Constriction Microchannels Using the DSMC Method, Journal of Microelectromechanical Systems, Vol. **14** (4), pp. 847-856.

[10] Whitfield, D. L., Janus, J. M., 1984, Three-dimensional unsteady Euler equations solution using flux vector splitting, AIAA Paper 84-1552.

[11] Wang, M., and Li, Z., 2004, Simulations for gas flows in microgeometries using the Direct Simulation Monte Carlo Method, International Journal of Heat & Fluid Flow, Vol. **25**, pp. 975–985.

[12] Chong, X., 2006, Subsonic Choked flow in microchannel, Physics of Fluids, Vol. **18**, 127104, 1-5.

[13] Chong, X., 2008, Private Communications.

[14] Fang, Y., Liou, W.W., 2002, Computations of the Flow and Heat Transfer in Microdevices Using DSMC with Implicit Boundary Conditions, Journal of Heat Transfer, Vol **124**, 338-345.

[15] Le, M., Hassan I., Esmail N., 2007, DSMC Simulation of Subsonic Flows in Parallel and Series Microchannels, Journal of Fluids Engineering, Vol. **128**, pp. 1153-1163.

[16] Karniadakis, G. E., Beskok, A., and Aluru, N., 2005, Micro flows and Nano flows: Fundamentals and Simulation, Springer-Verlag, New York.

[17] Graur, I. A., Meolans, J. G., Zeitoun, 2006, D. E., Analytical and numerical description for isothermal gas flows in microchannels, Microfluid and Nanofluid, Vol **2**, pp. 64-77.

[18] Darbandi, M., and Vakilipour, S., 2007, Developing Consistent Inlet Boundary Conditions to Study the Entrance Zone in Microchannels., Journal of Thermophysics and Heat Transfer, Vol. **21** (3) , pp. 596-607.